Biometals (2012) 25:711–723
DOI 10.1007/s10534-012-9529-7

Intracellular iron trafficking: role of cytosolic ligands

Maya Shvartsman · Z. Ioav Cabantchik

Received: 31 December 2011 / Accepted: 8 February 2012 / Published online: 17 February 2012

Abstract Iron acquired by cells is delivered to mitochondria for metabolic processing via pathways comprising undefined chemical forms. In order to assess cytosolic factors that affect those iron delivery pathways, we relied on microscopy and flow-cytometry for monitoring iron traffic in: (a) K562 erythroleukemia cells labeled with fluorescent metal-sensors targeted to either cytosol or mitochondria and responsive to changes in labile iron and (b) permeabilized cells that retained metabolically active mitochondria accessible to test substrates. Iron supplied to intact cells as transferrin–Fe(III) or Fe(II)-salts evoked concurrent metal ingress to cytosol and mitochondria. With either supplementation modality, iron ingress into cytosol was mostly absorbed by preloaded chelators, but ingress into mitochondria was fully inhibited only by some chelators, indicating different cytosol-to-mitochondria delivery mechanisms. Iron ingress into cytosol or mitochondria were essentially unaffected by depletion of cytosolic iron ligands like glutathione or the hypothesized 2,5 dihydroxybenzoate (2,5-DHBA) siderophore/chaperone. These ligands also failed to affect mitochondrial iron ingress in permeabilized K562 cells suspended in cytosol-simulating medium. In such medium, mitochondrial iron uptake was >6-eightfold higher for Fe(II) versus Fe(III), showed saturable properties and submicromolar $K_{1/2}$ corresponding to cytosolic labile iron levels. When measured in iron(II)-containing media, ligands like AMP, ADP or ATP, did not affect mitochondrial iron uptake whereas in iron(III)-containing media ADP and ATP reduced it and AMP stimulated it. Thus, cytosolic iron forms demonstrably contribute to mitochondrial iron delivery, are apparently not associated with DHBA analogs or glutathione but rather with resident components of the cytosolic labile iron pool.

Keywords Iron · Transport · Mitochondria · Fluorescence · Microscopy · Flow cytometry · Transferrin · Siderophores · Chelators

Abbreviations

AM	Acetomethoxyl ester
BDH2	Butyrate dehydrogenase2
BIPC	Carboxy-bipyridyl
BSO	Buthionine sulfoximine
CALG	Calcein green
2,5-DHBA	2,5-Dihydroxybenzoic acid
DMB	5,5′-Dimethyl-BAPTA
DFO	Desferrioxamine
DMEM	Dulbecco's modified eagle medium
DMSO	Dimethyl-sulfoxide
DMT1	Divalent metal transporter 1

Electronic supplementary material The online version of this article (doi:10.1007/s10534-012-9529-7) contains supplementary material, which is available to authorized users.

M. Shvartsman · Z. Ioav Cabantchik (✉)
Department of Biological Chemistry, The Alexander Silberman Institute of Life Sciences, The Hebrew University of Jerusalem, Edmond Safra Campus at Givat Ram, 91904 Jerusalem, Israel
e-mail: ioav@cc.huji.ac.il

FAS	Ferrous ammonium sulfate
FeS	Iron–sulfur cluster
F.U	Fluorescence units
GSH	Reduced glutathione
INT	Iodonitrotetrazolium
JC1	5,5′,6,6′-tetrachloro-1,1′,3,3′-tetraethylbenzimidazolylcarbocyanine iodide
LIP	Labile iron pool
MDR	Multidrug resistance
MRP	Multidrug resistance proteins
NTA	Nitrilotriacetic acid
PBS	Phosphate buffered saline
RPA	Rhodamine B-[(1,10-phenanthrolin-5-yl) aminocarbonyl benzyl ester
SIH	Salicyl isonicotinoyl hydrazide
TfFe	Transferrin–iron

Introduction

Iron is essential for a gamut of biochemical processes like oxygen binding, respiration, DNA synthesis and repair. As most of the cell metabolic iron is processed within mitochondrial compartments, it is of importance to understand how the metal is delivered to these organelles (Sheftel and Lill 2009). In most mammalian cells, physiological uptake of iron proceeds via endocytosis of circulating transferrin–iron (TfFe) complexes (Wang and Pantopoulos 2011) followed by steps of endosomal acidification and iron reduction via DMT1–STEAP3 (McKie 2005) or ZIP14 (Zhao et al. 2010; Liuzzi et al. 2006) reductase-associated transporters that lead to iron release and its translocation into the cell interior for metabolic utilization or storage (Wang and Pantopoulos 2011). Cytosolic iron utilization is seemingly associated with a pool of labile iron (LIP) (Kakhlon and Cabantchik 2002; Breuer et al. 2008) that comprises redox-active iron forms, exchangeable between metal binding ligands, while cell iron storage is linked to a catalyzed mineralization of the labile iron into ferritin protein iron cores (Arosio et al. 2009).

Hitherto, the mechanisms of cytosolic iron trafficking to mitochondria remain unresolved, largely due to technical difficulties in tracing transitory cell iron forms in real-time in different cell compartments. With the advent of fluorescent metalosensors that can be targeted to specific cell compartments such as cytosol and mitochondria, it has become possible to obtain kinetic information about iron ingress into these compartments using both physiological Tf–Fe and non Tf–Fe substrate forms. Our previous observations indicated that incoming TfFe accessed K562 mitochondria by multiple trafficking mechanisms (Shvartsman et al. 2010). These trafficking mechanisms are operationally defined as cytosolic chelator-sensitive and chelator-insensitive. While chelator-sensitive iron trafficking is allegedly mediated by endogenous components of the cytosolic labile iron pool (Kakhlon and Cabantchik 2002; Zhan et al. 1990), chelator-insensitive trafficking is associated with occluded iron forms that are either complexed to cytosolic high-affinity iron-binding ligands (Shi et al. 2008; Devireddy et al. 2010) or sequestered within endosomes (Sheftel et al. 2007). In the current study, we aimed to assess whether the prevailing cytosolic metal ligands can mediate or affect iron delivery to mitochondria. Previous studies with isolated mitochondria have addressed this issue by using radiolabeled iron and various cytosolic ligands that can complex iron (Weaver and Pollack 1990; Weaver and Pollack 1990). The complexes were assessed in terms of their ability to support radiolabeled heme synthesis, which was taken as a measure of mitochondrial iron uptake and processing, but not of transport per se. In this work we used K562 erythroleukemia cells for monitoring iron ingress into cytosol and mitochondria and for assessing the effect of cytosolic factors on intracellular iron traffic. We selected these erythroid–myeloid cells because they express an abundant number of functional transferrin receptors and display active iron and heme metabolism (Klausner et al. 1983), including inducible hemoglobin synthesis (Andolfo et al. 2010). Moreover, these cells have a demonstrable ability to acquire both physiological TfFe (Klausner et al. 1983) and non-Tf iron complexes (Lane and Lawen 2008) and can be used for on line monitoring of iron ingress into cytosol and mitochondria by real time fluorescence (Breuer et al. 1995; Shvartsman et al. 2010). For that purpose we labeled the cells with fluorescent metalosensors: (a) the green fluorescent calcein green (CALG) as described by Epzstejn et al. (1997) for assessing cytosolic labile iron and (b) the red fluorescent rhodamine B-[(1,10-phenanthrolin-5-yl) (RPA) aminocarbonyl benzyl ester, as described by Petrat et al. (2002) for labeling mitochondria. The assessment of cytosolic factors that

affect iron uptake into mitochondria were complemented with studies done on digitonin-permeabilized cells, which lack the plasma membrane barrier but retain functional mitochondria (Nishikawa et al. 1984). These experimental systems allowed us to determine the kinetic parameters of iron ingress to mitochondria, as well as the substrate specificity of the mitochondrial iron import machinery.

Experimental procedures

Reagents

All reagents were obtained from Sigma-Aldrich Israel, unless otherwise indicated. Human fully saturated TfFe was obtained from Kamada Industries (Ness Ziona, Israel). The cytosolic metalosensor CALG acetomethoxyl-ester (CALG-AM) and the JC1 mitochondrial potentiometric probe were obtained from Molecular Probes, Eugene, OR. The mitochondrial metalosensor RPA was a kind gift of Prof. U. Rauen, Essen. SYBR-Green was obtained from Applied Biosystems. shRNA plasmid (sc-89195-SH) against human BDH2 was obtained from Santa-Cruz Biotechnology.

Cell culture

K562 human erythroleukemia cells were cultured in Dulbecco's modified eagle medium, with 4.5 gr/l glucose, foetal bovine serum, antibiotics and L-glutamine (10, 1 and 1% respectively). All cell culture reagents were obtained from Biological Industries, Kibbutz Beit HaEmek, Israel.

Iron uptake measurements and calculations

K562 cells were taken from a logarithmically growing culture and the cell density adjusted to 1–2 $\times$ 10^6 cells/ml and maintained throughout different treatments at constant density. Cells were resuspended in warm DMEM–Hepes pH 7.3 medium and labeled with RPA 1 μM for 15 min at 37°C, in presence of 50 μM desferrioxamine (DFO, from Novartis, Basel) chelator to bind contaminating iron in the medium. Cells were subsequently resuspended in DMEM–Hepes medium with or without CALG-AM 0.125 μM for 10 min at 37°C, washed in DMEM–Hepes and analyzed or permeabilized with digitonin 12.5 μM and then analyzed in a iCyt flow cytometer (iCyt Mission Technology, Champaign, IL). After attainment of a stable fluorescence signal iron was added to cells at 5–10 μM final concentrations either as TfFe, ferric-nitrilotriacetic acid (NTA) (1:1) or ferrous ammonium sulfate (FAS). In order to obtain the kinetic parameters of iron uptake, cell samples were taken either at 15 min intervals for up to 1 h or a single point was taken at 30 min. CALG fluorescence was recorded with the FL1 channel using the fluorescein settings (λem 520 nm) and RPA fluorescence was simultaneously recorded with the FL2 channel using rhodamine settings (λem 610 nm). Fluorescence changes by added iron were converted into changes in labile iron concentrations in cytosol and mitochondria as previously described (Shvartsman et al. 2010 and supplemental Experimental procedures).

Cell permeabilization

K562 cells, stained with metalosensors as described above, were resuspended in a 37°C permeabilization buffer (KCl 120 mM, Hepes 10 mM pH 7.22, Na_2HPO_4 5 mM, $MgCl_2$ 1 mM, $CaCl_2$ 1 μM, DFO 1 μM, succinate 2 mM (Shvartsman et al. 2007), digitonin 12.5 μM) for 30 s, washed with the same permeabilization buffer without digitonin. Cell permeabilization was confirmed by loss of originally loaded CALG and mitochondrial integrity was confirmed in a separate set of experiments by monitoring the signal of the potentiometric mitochondrial probe JC1.

For determination of kinetic parameters of iron ingress to permeabilized K562 cells, RPA-labeled cells were exposed to 0–20 μM Fe(II) as FAS or Fe(III) as Fe-NTA and RPA fluorescence was monitored for 30–60 min at 5 min intervals by flow cytometry. Initial iron ingress rates were calculated by linear regression of RPA quenching and expressed as fluorescence units quenched (F.U.) per min. Maximal iron ingress rates V_{max} and apparent half saturation constants $K_{1/2}$ were calculated by non-linear least square regression ($n = 3$ independent experiments) by Origin 8 (OriginLab Corp., MA).

Generation of K562 BDH2i clones

K562 cells, plated to the density of 0.5 $\times$ 10^6 cells/ml in complete growth medium were transfected with 2 μg BDH2 shRNA plasmid (sc-89195-SH, Santa Cruz Biotechnology), with the aid of TransIT-LT1

transfection reagent (Myrus, WI) according to manufacturer's instructions. After 48 h, the medium was replaced with puromycin 1 μg/ml-containing medium. Puromycin selection continued for a month. The remaining surviving colonies were propagated in complete medium with 0.5 μg/ml puromycin and taken to characterization or frozen.

RT-PCR for BDH2

Total RNA was extracted from 10^7 cells with RNeasy Plus Mini Kit (Qiagen) and reverse-transcribed with SuperScript First-Strand synthesis system (Invitrogen) according to manufacturer's instructions. 2 μg of total cDNA were taken to real-time PCR with SYBR-Green mix (Applied Biosystems). The extent of BDH2 silencing was calculated by comparative ΔC_t method, with normalization on GAPDH transcript levels. BDH2 primers (Sigma) were 5′→3′ GCAACTGTGTGTGC CCAGGAAC (forward) and AAGGGCCTGCCTTCC TTCCCA (reverse). GAPDH primers were 5′→3′ TAAATTGAGCCCGCAGCCT (forward) and AATC CGTTGACTCCGACCTTC (reverse). SYBR Green fluorescence was measured with the aid of ABI PRISM 7900 HT and the data analyzed by SDS 2.3 software (Applied Biosystems).

Isolation of mitochondria and enzyme assays

K562 cells (0.5–1 × 10^7 cells) were washed with phosphate buffer solution (PBS) buffer (Na_2HPO_4 16.2 mM, NaCl 150 mM, NaH_2PO_4 3.8 mM, pH 7.3) and lysed in ice-cold lysis buffer (Tris 20 mM pH 7.4, sucrose 250 mM, digitonin 0.007%, protease inhibitors) through a syringe and 21G needle. This lysis method (Machida et al. 2006) proved rapid, reproducible and efficient for mitochondrial isolation. Mitochondrial and cytosolic fractions were obtained by differential centrifugation at 4°C (1,000×g × 5 min to remove nuclei and unbroken cells, followed by 4,000×g × 10 min to obtain mitochondria-enriched pellets, and by 16,000×g × 10 min, to obtain particle-free cytosolic fractions). The quality of the fractions was assessed by immunoblotting with anti-actin and anti-VDAC antibodies (Sigma-Aldrich, Israel).

For the aconitase assay, the rate of NADPH formation was monitored by fluorescence at λexc 345 nm, λem 550 nm, as previously described (Kakhlon et al. 2008). The reaction buffer was: Tris 50 mM pH 7.4, NADP 0.2 mM, Na-citrate 2.5 mM, $MnCl_2$ 0.5 mM, isocitrate dehydrogenase 4 units/ml. For the succinate dehydrogenase assay, the rate of iodonitrotetrazolium (INT) reduction was monitored by absorbance increase at 500 nm, as previously described (Munujos et al. 1993). Fluorescence or absorbance was measured with a Tecan SAFIRE instrument (Neotec, GmbH, Austria). The initial rate of fluorescence or absorbance increase was normalized on total protein, quantified by bicinchoninic acid method (Pierce Chemical Company, Rockford, IL).

Cellular ATP quantification

ATP in cellular extracts was quantified by luciferase assay with a bioluminescent somatic cell assay kit (Sigma address). Luminescence was measured with a Modulus luminometer (Turner BioSystems, Sunnyvalee, CA address) s per the manufacturer instructions.

Cellular glutathione (GSH) depletion, and determination of GSH levels

K562 cells, plated at 1 × 10^6 cells/ml density were incubated with buthionine sulfoximine (BSO) 50 μM for 24 h in complete growth medium, as previously described (Crook et al. 1986). For TfFe trafficking studies, cells were washed with warm DMEM–Hepes pH 7.2 medium, labeled with metalosensors and taken to flow cytometry experiments, as described above. For determination of intracellular GSH levels, 8 × 10^6 cells were washed in ice-cold PBS and lysed on ice by mechanical shearing through a syringe and 21G needle, in a lysis buffer pH 7.4 containing KH_2PO_4 (16 mM), K_2HPO_4 (84 mM), EDTA (1 mM), Triton X (0.1%) and sulfosalicylic acid (0.6% w/v). After protein precipitation, lysates were taken to a 5,5′-dithio-bis(2-nitrobenzoic acid) assay on a 96-well plate, as previously described (Rahman et al. 2006). The rate of absorbance increase at 412 nm was normalized by the number of cells in a sample.

Siderophore-iron complex formation and stability

2,3 and 2,5 dihydroxybenzoic acid (DHBA) were solubilized to 10 mM in ethanol or DMSO and mixed with $FeCl_3$ in a 10:1 siderophore:Fe stoichiometry as described by Bao et al. (2010). Absorbance spectra from 350 to 750 nm were recorded on an Agilent 8453 UV spectrophotometer. For stability assays, the complexes were

diluted tenfold in the original organic solvent or in a range of aqueous buffers and absorbance spectra were recorded. The aqueous buffers were: HBS (Hepes 20 mM pH 7.3, NaCl 150 mM); Tris 50 mM pH 7.3; PBS (Na_2HPO_4 16.2 mM, NaCl 150 mM, NaH_2PO_4 3.8 mM, pH 7.3) and cell permeabilization buffer without digitonin and succinate (KCl 120 mM, Hepes 10 mM pH 7.22, Na_2HPO_4 5 mM, $MgCl_2$ 1 mM, $CaCl_2$ 1 μM, DFO 1 μM).

Results

Initial characterization of iron uptake into cell compartments in intact and permeabilized K562 cells

Real-time monitoring of iron ingress into mitochondria and cytosol relied on the use of fluorescent metalosensors that are targeted to these compartments, RPA for mitochondria on a potentiometric manner (Petrat et al. 2002) and CALG for cytosol, by intracellular hydrolysis of a permeant acetomethoxy precursor CALG-AM (Epzstejn et al. 1997). Confocal fluorescence microscopy was used for probe cell localization (Fig. 1a) and flow cytometry for tracing with time metalosensor quenching by incoming iron (Fig. 1b). Following loading, the cells showed variable degrees of spontaneous leakage, which for CALG could be largely overcome by addition of the multidrug resistance pump (MRP) blocker probenecid (Shvartsman et al. 2010) while for RPA the leakage over time was probenecid-insensitive (Fig. 1c) and had to be subtracted for subsequent net-iron ingress calculations. The presence of the MRP blockers did not affect the initial labeling of cells by RPA or CALG, or CALG responsiveness to added iron, indicating no significant interference of the blocker with the cytosolic labile iron

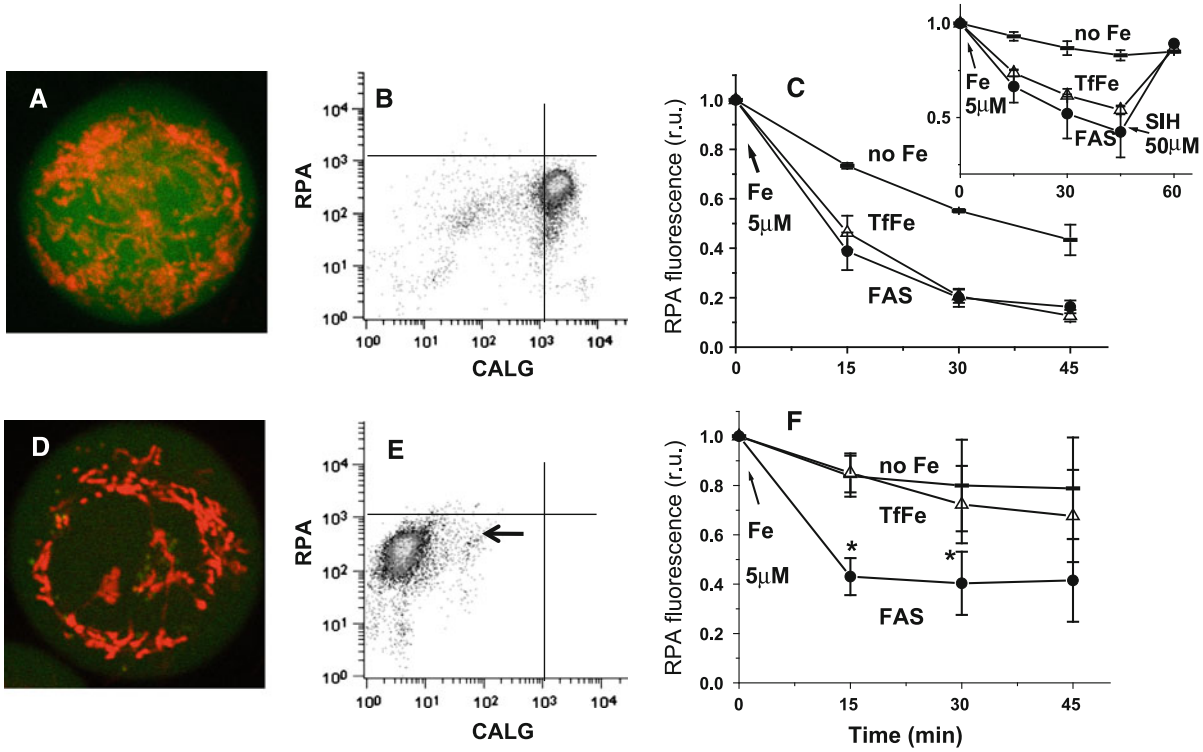

Fig. 1 Localization and quenching of fluorescent metalosensors in intact and permeabilized cells K562 cells stained with RPA and CALG metalosensors are depicted as fluorescence confocal images (**a**) and flow cytometry density plots (**b**): RPA-ordinate and CALG-abscissa. **c** Normalized values of RPA and CALG (*inset*) fluorescence obtained by flow cytometry in K562 cells, were plotted as a function of time (mean ± SD, $n = 3$). Fluorescence signals were monitored in the absence (no Fe) or presence of 5 μM iron (TfFe or ferrous ammonium sulfate, FAS). CALG quenching by iron was reversed with the permeant chelator SIH (50 μM) added at the indicated time. Fluorescence confocal images of digitonin-permeabilized K562 labeled cells (**d**) and their flow cytometry density plot (**e**): RPA-ordinate and CALG-abscissa. **f** Values of RPA fluorescence obtained by flow cytometry in digitonin-permeabilized cells, were plotted as a function of time (mean ± SD, $n = 3$, $^*P = 0.003$ compared to no Fe, Student's t test)

pool and mitochondrial membrane potential. A supplementation of 5 μM iron as physiological TfFe or as permeant model substrate FAS, evoked time-dependent quenching of both cytosolic and mitochondrial fluorescence (Fig. 1c). That the quenching of cell cytosol-associated fluorescence results from iron ingress into cells we deduce from the fact those changes occur only when cells are supplemented with appropriate iron sources and that those changes can be reversed by addition of permeant high-affinity chelators like SIH (Fig. 1c, inset) but not of poorly permeant ones like DFO (Kakhlon and Cabantchik 2002). On the other hand, permeabilization of K562 cells with 12.5 μM digitonin released most of the cytosolic CALG (Fig. 1d, e, arrow) while sparing mitochondrial integrity and preserving their functionality (Fig. 1d), as reflected in the retention of RPA signal (Fig. 1e). Unlike supplementation of TfFe to permeabilized cells that produced essentially no change in RPA fluorescence, iron supplied as FAS did evoke fast and marked changes in RPA, indicating swift Fe(II) access to the mitochondria interior (Fig. 1f). In both experimental settings of iron delivery from different sources, namely using physiological TfFe and non-physiological iron complexes, the presence of CALG in the cytosol did not affect the delivery of iron to mitochondria (Shvartsman et al. 2007; Shvartsman et al. 2010).

Role of cytosolic iron ligands on iron ingress into K562 cell compartments

Intracellular chelation

In order to assess whether iron supplied to cells is delivered to mitochondria via the cytosolic compartment, we first assessed the effects of iron chelators preloaded into cells on iron ingress into both cytosol and mitochondria. The chelators were preloaded into cells before their staining with metalosensors, by 10 min incubation with their acetomethoxyl-ester-derivatives (5,5′-dimethyl BAPTA-AM (DMB-AM) 50 μM or carboxy-bipyridyl (BIPC-AM) 25 μM) which diffuse through the plasma membrane and undergo hydrolysis by cytosolic esterases in a manner similar to CALG-AM (Shvartsman et al. 2007, 2010). The concentrations of DMB and BIPC attained in cells were in the range of 2–3 and 10–12 mM, respectively, measured as described in Shvartsman et al. 2007. Either of the two chelators loaded, effectively blocked the raise in cytosolic labile iron evoked by addition of 5 μM TfFe or FAS, as reflected in cytosolic CALG quenching (Fig. 2a). However, whereas BIPC fully blocked also iron delivery to mitochondria, DMB inhibited the latter only partially (Fig. 2b). We interpret these results as indicative for the operation of two different mechanisms involved in iron delivery to mitochondria, which we denote as chelator-sensitive and chelator-resistant. The chelator-sensitive mechanism is associated with the cytosolic LIP, revealed with CALG and redox active in the sense that is susceptible to relatively mild chelators of both iron II and III (such as DMB and CALG) and of iron (II) (such as BIPC). The chelator-resistant mechanism

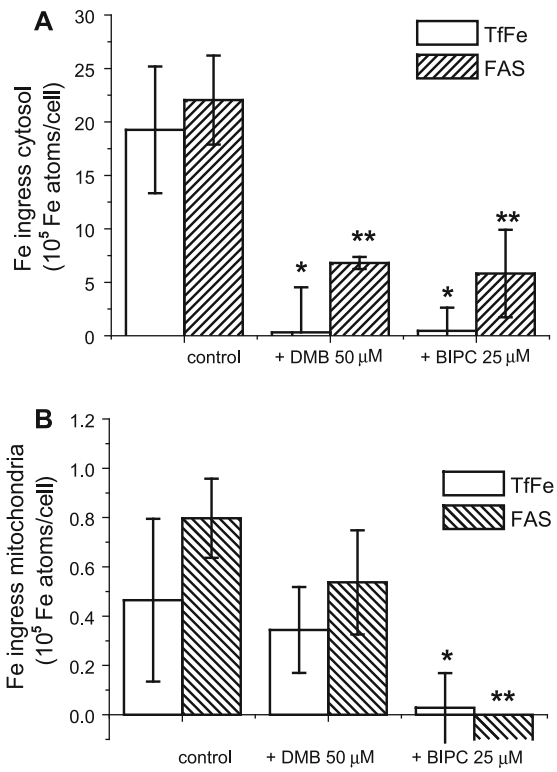

Fig. 2 Effect of cytosolic iron chelators on iron ingress into cell compartments. Cells labeled with CALG and RPA were preloaded or not (*control*) with cytosolic iron chelators 5,5′-dimethyl-BAPTA (DMB, 50 μM) or carboxybipyridyl (BIPC 25 μM). Iron (5 μM) was supplemented as TfFe (*white bars*) or FAS (*hatched bars*) and fluorescence was analyzed by flow cytometry as in Fig. 1. *Bars* denote cytosolic (**a**) and mitochondrial (**b**) iron ingress after 30 min incubation of intact K562 cells with supplemented iron. The values of iron taken up by cells after 30 min incubation with iron were calculated as described in Experimental procedures (mean ± SD, n = 3, * and $^{**}P < 0.05$ compared to control, ANOVA)

is apparently insensitive to CALG and DMB, but is blocked by BIPC, indicating that it is of higher apparent iron affinity and/or of different accessibility than CALG or DMB.

Cell reductive environment

As reduced glutathione GSH was proposed to act as a major component of cellular labile iron pools (Hider and Kong 2011), we assessed whether depletion of intracellular GSH levels might affect those putative pools and thereby iron delivery to cytosol and mitochondria. Though BSO pretreatment of K562 cells led to a major reduction (0.14 ± 0.003 nmol/10^6 cells in control untreated cells compared to 0.0003 ± 0.0001 nmol/10^6 cells, >90% reduction) in intracellular GSH levels, it failed to reduce iron ingress derived from TfFe either in the cytosol (Fig. 3a) or in mitochondria (Fig. 3b). These results indicate that GSH might not be directly involved or play an essential role in iron delivery to mitochondria.

DHBA as putative chaperone of mitochondrial iron

The 2,5 analog of the 2,3 dihydroxybenzoate DHBA bacterial siderophore was recently proposed to act as a mammalian siderophore that is conserved in evolution and essential for iron trafficking to mitochondria and synthesis of heme (Devireddy et al. 2010). In order to assess the possible contribution of 2,5-DHBA we first attempted to follow the original studies of 2,5-DHBA depletion and assess its possible effects on iron metabolism in K562 cells. We generated for that purpose K562 clones, shRNA-silenced for the proposed siderophore-synthesizing enzyme β-hydroxybutyrate dehydrogenase 2 (BDH2), also known by the name DHRS6 (Devireddy et al. 2010; Guo et al. 2006). Three different clones that express (by RT-PCR) 23–35% of the wild type BDH2 levels were selected for the present study (Fig. 4a). We found that the cellular ATP levels that are indicative of normal mitochondrial functionality and energy status were essentially unaltered in the 3 clones (Fig. 4b). Cell morphology and viability were also uncompromised in the clones (Shvartsman and Cabantchik, unpublished observations), and only one, cl D, displayed a statistically significant reduction in mitochondrial and cytosolic aconitase activity (Fig. 4c). We were not in a position to assess directly the mitochondrial

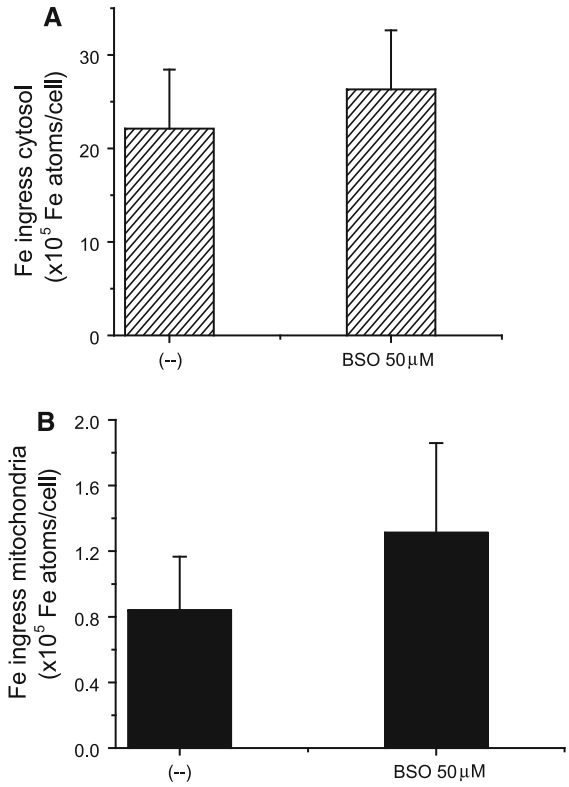

Fig. 3 Effect of cell GSH levels on iron access into cell compartments. K562 cells treated or not with 50 μM buthionine sulfoximine (BSO) for 24 h, (in order to deplete intracellular GSH levels by >90%), were loaded with CALG (**a**) and RPA (**b**) and exposed for 30 min to 5 μM TfFe. Cell fluorescence was analyzed by flow cytometry and values of ingress calculated as described in Fig. 2. (mean ± SD, $n = 3$; no significant difference observed at $P < 0.05$, with Students's t test)

membrane potential because in the process of clone selection for puromycin resistance, the K562 cells acquired enhanced multidrug resistance (MDR) properties that limited the use of potentiometric dyes. However, by using the MDR blocker verapamil 20 μM, we revealed with JC1 essentially similar red/green ratio fluorescence in clones and WT, indicating similar mitochondrial membrane potentials (Shvartsman and Cabantchik, unpublished observations). Accordingly, real-time monitoring of iron delivery (from TfFe) to cytosol and mitochondria, showed non-statistically significant decrease of iron uptake to either cell compartment in clone D as compared to wild type (Fig. 4d). Moreover, hemoglobin synthesis resulting from induction by sodium butyrate or hemin, was also not reduced in any of the clones studied (data not shown).

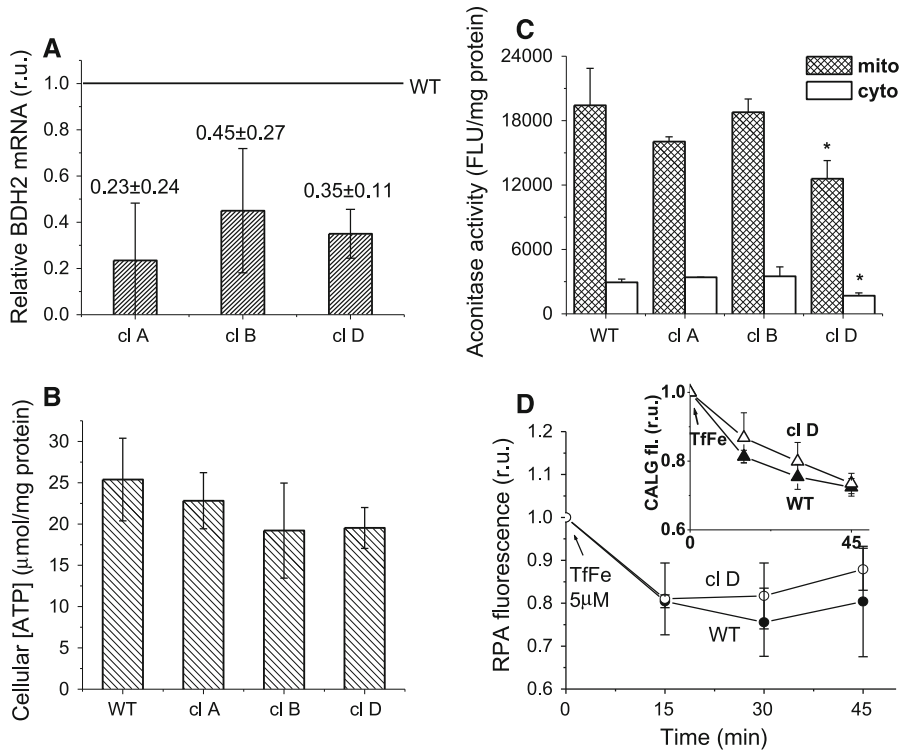

Fig. 4 Properties of K562 cells following suppression of the BDH2 gene. The BDH2 gene that codes for the enzyme involved in 2,5-DHBA synthesis was suppressed by shRNA transfection of K562 cells as described in Experimental procedures. **a** *Bars* denote relative mRNA levels of BDH2 in K562 cells untransfected (WT) or transfected with BDH2 shRNA, as determined by RT-PCR (mean ± SD, $n = 3$). BDH2 mRNA levels were normalized to GAPDH. **b** *Bars* denote total cellular ATP levels in µmol/mg total protein quantified in WT and BDH2-silenced clones by luciferase assay (mean ± SD, $n = 5$). **c** *Bars* denote mitochondrial (*hatched*) and cytosolic (*white*) aconitase activity in WT and clones, normalized by mg total protein (mean ± SD, $n = 4$, $^*P < 0.05$ compared to WT, ANOVA). **d** Iron ingress into cells loaded with mitochondrial RPA and cytosolic CALG (*inset*) observed following incubation with 5 µM TfFe in WT (*filled shapes*) and clone D (*empty shapes*) cells. Fluorescence measured by flow cytometry was analyzed as in Fig. 1 and the depicted iron *ingress values* represent mean ± SD, $n = 3$

Since BDH2 silencing apparently had no effect on iron trafficking to mitochondria in K562 cells or on mitochondrial properties, we also assessed the possibility that the proposed 2,5-DHBA might be endowed with insufficiently high iron binding capacity and complex stability for competing with other cytosolic ligands like CALG or DMB. Qualitatively similar to the bacterial siderophore analog, 2,3-DHBA (Fig. 5a), the putative mammalian 2,5-DHBA siderophore could be shown spectroscopically to bind iron in an organic/aprotic solvent (Fig. 5b). A 600 nm absorbance peak corresponded to the association of iron with dihydroxybenzoates in organic or aprotic solvents, which increased progressively with increasing iron concentrations (Fig. 5a, b). Dilution of the preformed 2,3-DHBA:$FeCl_3$ complexes in HEPES-buffered pH 7.3 phosphate-free solutions (pH changed by no more than 0.1 units) shifted the absorbance peak from 600 to 520 nm, possibly indicating a change in complex stoichiometry and/or composition (Figs. 5c, S1). These complexes apparently dissociate in physiological phosphate containing media as reflected in the disappearance of the identifying absorption peaks (Supplement Fig. S1) suggesting that phosphates destabilize the complex. As the 2,5-DHBA putative mammalian siderophore failed to retain iron in physiological pH 7.3 solutions (Figs. 5c, S1) regardless of the presence of phosphates, we deduce that 2,5-DHBA alone cannot stably bind iron in physiological conditions. Moreover, 2,5-DHBA failed to compete for iron with CALG under any experimental condition used in cells or in the test tube, indicating that by itself, the compound had no significant affinity for iron in physiological media (Shvartsman and Cabantchik, unpublished observations).

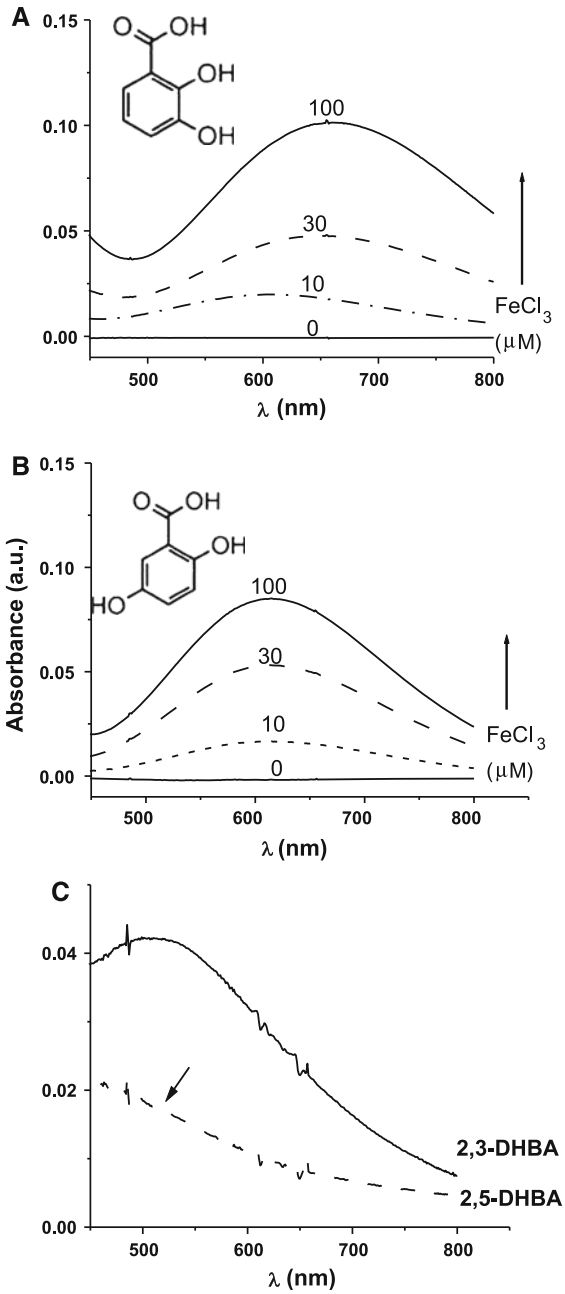

Fig. 5 Iron binding by dihydroxybenzoates and complex stability in aqueous solution Absorbance spectra of the bacterial siderophore 2,3-DHBA (**a**) and the proposed mammalian 2,5-DHBA siderophore (**b**) were recorded by UV spectrophotometry. The spectra were taken following titration of the siderophore (100 μM in DMSO) with increasing concentrations (0–100 μM) of $FeCl_3$ (similar data were obtained with methanol solutions, not shown). **c** Represents spectra of 10:1 DHBA:Fe complexes formed in DMSO that were diluted tenfold in HEPES 20 mM pH 7.3 buffer. The disappearance of the absorbance peak characteristic of the 2,5-DHBA:Fe complex (*arrow*) denotes its dissociation in aqueous medium

Effect of cytosolic iron-binding ligands on iron access to mitochondria in digitonin-permeabilized cells

In order to assess the ability of mitochondria to import iron from components of the cytosolic labile iron pool, we used digitonin-permeabilized K562 cells in which the mitochondria were RPA labeled, as described in Fig. 1. The permeabilized cells were exposed to 0–20 μM Fe(II) or Fe(III) salts supplemented to cytosolic-like media rich in K (120 mM), Mg (1 mM), Ca (1 μM), phosphate (5 mM), and succinate (2 mM). The cytosolic medium was also supplemented with 1 μM DFO in order to eliminate traces of iron that contaminated the media components. The presence of DFO prevented entry of contaminating metal into RPA-laden mitochondria prior to addition of the test iron salts. The values of initial iron uptake (V_0) determined as described previously for intact cells (Shvartsman et al. 2010) were used for constructing the Michaelis–Menten plot (Fig. 6) and calculating the kinetic parameters by non-linear regression analysis (Table 1). For the latter we used the effective iron concentrations attained after addition of iron to the DFO-containing solution. The data depicted in Fig. 6 and analyzed in Table 1 indicate that mitochondria are endowed with a high affinity import system for Fe(II) and that the presence of physiological concentrations of GSH did not significantly affect the Fe(II) uptake parameters, although they improved somewhat the uptake when iron was given as Fe(III). Likewise, the presence of AMP in Fe(III) but not Fe(II)-containing medium (Table 1) significantly raised iron uptake as reflected in V_{max} values. On the other hand, ADP and ATP did not significantly affect either kinetic parameter of Fe(II) uptake in cytosolic-like medium. This study indicates that Fe(II) in cytosolic-like medium can largely sub-serve mitochondrial iron import, that the prevailing adenine nucleotides do not affect Fe(II) uptake but both AMP and GSH can significantly enhance the uptake when iron is in the Fe(III) state.

Discussion

The present study deals with the cellular steps that follow iron uptake by K562 erythroleukemia cells as reflected in the cytosolic labile pool and in mitochondria. These steps were assessed by flow cytometry and

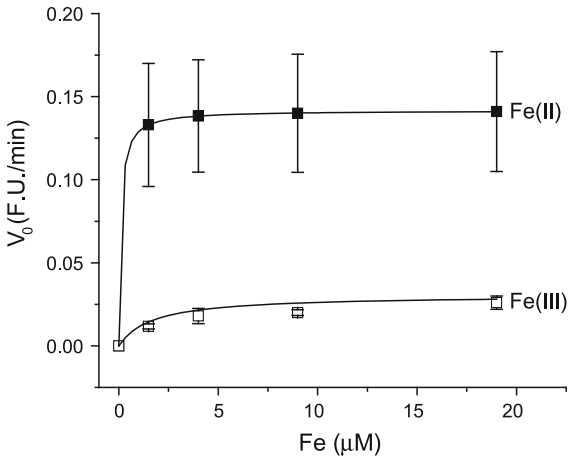

Fig. 6 Fe(II) and Fe(III) ingress kinetics into mitochondria of digitonin-permeabilized K562 cells loaded with RPA. The initial rates (V_0) of iron access to RPA-labeled cells were obtained by time-dependent measurements of fluorescence for different iron concentrations supplied as Fe(III) (FeNTA, *empty square*, $n = 3$) or Fe(II) (FAS, *filled square*, $n = 3$, average ± SD). Fluorescence measurements were done by flow cytometry as described in Experimental procedures. The *lines* were calculated by non-linear square analysis of hyperbolic curves and the derived kinetic parameters are given in Table 1

live fluorescence imaging with the aid of fluorescent metalosensors targeted to the respective compartments (Fig. 1). Using these methodologies on K562 cells we have recently shown that most of the iron taken up physiologically from circulating TfFe or pathophysiologically from non-TfFe, is initially detected in the cytosol and a minor but significant fraction also in mitochondria (Shvartsman et al. 2007, 2010). These studies in conjunction with others that involved the use of inhibitors of endosomal dynamics on iron delivery from circulating TfFe to mitochondria and its differential susceptibility to intracellular chelators led us to propose the operation of diverse cytosol-mitochondria routes of iron traffic (Shvartsman et al. 2010). In this work we determined that a similar diversity of cytosolic routes to mitochondria is detected when iron is supplied to cells as non-TfFe (Fig. 2), suggesting a convergence of cytosolic iron pools derived from uptake of TfFe and non-TfFe iron, as pictorially depicted in Fig. 7. This has led us to inquire about the nature of the cytosolic iron pools in terms of their ability to furnish iron to mitochondria, as predicted from our earlier studies (Shvartsman et al. 2010).

We first focused on the possible involvement of cytosolic iron binding ligands in iron trafficking, like the highly prevalent GSH (Hider and Kong 2011) and the recently proposed mammalian siderophore 2,5-DHBA (Devireddy et al. 2010). We found that >90% depletion of GSH in intact K562 cells did not affect iron uptake (from TfFe) into cytosol or mitochondria of intact cells (Fig. 3) and neither did GSH supplementation affected

Table 1 Kinetic parameters of iron ingress to mitochondria of permeabilized K562 cells in the presence of cytosolic ligands

Substrate	Added ligand [mM]	$K_{1/2app}$. (μM)	V_{max} (F.U./min)	V_0 at 1.5 μM Fe (F.U./min)
Fe(II)	None	0.110 ± 0.049	0.142 ± 0.035	0.133 ± 0.037
	ATP [1]	0.359 ± 0.232	0.163 ± 0.013	0.131 ± 0.027
	ADP [1]	N.D.	N.D.	0.140 ± 0.031
	AMP [1]	0.349 ± 0.182	0.134 ± 0.007	0.118 ± 0.021
	GSH [1]	0.110 ± 0.035	0.150 ± 0.002	0.144 ± 0.011
Fe(III)	None	1.977 ± 0.604*	0.030 ± 0.002*	0.012 ± 0.002
	ATP [1]	15.494 ± 12.199	0.023 ± 0.011	0.003 ± 0.002**
	ADP [1]	7.179 ± 5.045	0.029 ± 0.008	0.007 ± 0.006
	AMP [1]	2.870 ± 0.872	0.041 ± 0.004**	0.017 ± 0.006
	GSH [1]	1.131 ± 0.219	0.040 ± 0.002**	0.027 ± 0.001

The values of the apparent $K_{1/2}$ ($K_{1/2app}$) and V_{max} of Fe(II) and Fe(III) ingress to mitochondria of permeabilized cells were calculated by non-linear least-square analysis of data obtained as described in Fig. 6, in the absence and presence of different ligands added to cytosol-like media. The values are given as mean ± SD, $n = 3$; statistical significant differences $P < 0.05$ (ANOVA) between $K_{1/2\ app}$ and V_{max} parameters of Fe(II) versus Fe(III) ingress are denoted * and the respective ones for Fe(III) are denoted **. F.U. represents a fluorescence unit that is equivalent to 30 μM iron, calculated as described in the supplement following previously described studies. (Shvartsman et al. 2007, 2010)

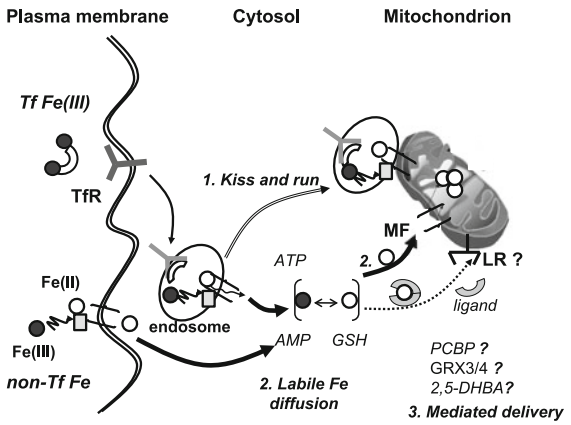

Fig. 7 Iron trafficking mechanisms in K562 cells In K562 cells the uptake of either TfFe by endocytosis or non-TfFe by transporters such as DMT1 or ZIP14 (linked to ferric reductases) is primarily reflected in the cytosol as appearance of labile iron. The proposed "kiss and run" pathway (*1*) involving direct transfer of iron from TfFe-containing endosomes to mitochondria (Sheftel et al. 2007) might contribute to iron delivery to mitochondria, but apparently to a limited extent, whereas cytosolic diffusion of labile iron complexes (*2*), which involves both iron redox states and the participation of cytosolic ligands (this work) is seemingly the most prevalent in K562 cell. The possible contribution of a mediated delivery pathway involving high-affinity ligand (*3*) like the 2,5-DHBA siderophore proposed by Devireddy et al. 2010, or a chaperone associated with glutaredoxins (Grx3/4), as suggested by Mühlenhoff U et al. 2010, or a PCBP-analog (Shi et al. 2008) as proposed for transfer of iron to ferritin, they all remain to be established. The major mitochondria import agency of Fe(II) would seem to be mitoferrin (MF) (Paradkar et al. 2009), which seemingly can acquire the metal from resident cytosolic sources, as those presented in the present study. The possibility that either MF or other mitochondrial transporters/receptors (LR) can also acquire iron from nucleotide–Fe(III) complexes or other high affinity iron(III) ligands (Weaver and Pollack 1990), remains to be established

Fe(II) uptake into mitochondria of permeabilized cells (Table 1). The latter however showed a small but significant enhancement of Fe(III) mitochondrial uptake by added GSH, suggesting a (direct or indirect) role of GSH in maintaining some reduced iron in permeant form, but not a key role in mediating iron trafficking to mitochondria. Studies with the putative mammalian siderophore 2,5-DHBA, which was proposed to be essential for iron trafficking to mitochondria in murine erythroleukemia cells and zebrafish (Devireddy et al. 2010), were carried out here with K562 human erythroleukemia cells. Silencing the cytosolic siderophore-synthesizing enzyme BDH2 failed to reduce: (a) TfFe trafficking to mitochondria, (b) activity of mitochondrial respiratory complexes, cell ATP levels and mitochondrial membrane potential and (c) inducible hemoglobin synthesis. Moreover, our spectroscopic studies of 2,5-DHBA indicate a very low ability of this putative siderophore to bind iron in physiological conditions and virtually no ability to compete with cytosolic agents like ATP, ADP, AMP or inorganic phosphate, let alone with metal binders like CALG or DMB. Likewise, this siderophore had no detectable effect on cell iron trafficking in intact or permeabilized cells. We therefore conclude that by itself, 2,5-DHBA is not likely to play a role in iron trafficking to mitochondria. The possibility that the 2,5-DHBA moiety might be a component of a more complex siderophore or chaperone associated with iron metabolism remains at this point speculative.

The involvement of adenine nucleotides in cytosolic binding of iron and transfer to mitochondria in mammalian cells has been proposed earlier (Weaver et al. 1989; Weaver and Pollack 1990) and reassessed in this work in permeabilized cells in terms of iron ingress kinetics into mitochondria exposed to cytosol-like medium. The analysis revealed the operation of a high affinity import machinery of iron(II) that was unaffected by added nucleotides to any significant extent (Table 1). On the other hand, when iron was offered as Fe(III), ATP or ADP repressed mitochondrial iron uptake while AMP enhanced it, similar to what was observed by Weaver and Pollack (1989, 1990) and accordance with the relative binding affinities of nucleotide phosphates for Fe(III) (Weaver and Pollack 1989, 1990; Shalev and Hebbel 1996). The fact that mitochondria can acquire Fe(II) from physiological components of the cytosol in the presence or absence of physiological nucleotides or redox modulators such as GSH suggest that they are endowed with a robust- transport system for Fe(II). Their ability to take up iron also from Fe(III) complexes is considerably more restricted, as reflected in the kinetic parameters and its susceptibility to nucleotides. To what extent all those modalities of uptake converge to the only identified mitoferrin iron transporters (Shaw et al. 2006; Paradkar et al. 2009) remains to be established. Since the cytosolic concentration of labile iron lies within the submicromolar range (Epzstejn et al. 1997), and since knockdown of mitoferrins in mammalian cells only reduces mitochondrial iron uptake by 84% (Paradkar et al. 2009), we assume that mitochondria harbor a range of Fe(II)

and Fe(III) uptake systems. While the high-affinity uptake systems for Fe(II) predominantly supply iron for heme and FeS-cluster synthesis (Mühlenhoff et al. 2002; Lange et al. 1999), the uptake systems for Fe(III) (Weaver et al. 1990) have a compensatory role. The systems for mitochondrial iron uptake might include transporters and receptors for siderophores (Devireddy et al. 2010) or chaperones (Shi et al. 2008), to accommodate with all modalities of intracellular iron trafficking.

Acknowledgment We wish to thank Dr. N. Melamed-Book for assistance with confocal microscopy.

References

Andolfo I, De Falco L, Asci R, Russo R, Colucci S, Gorrese M, Zollo M, Iolascon A (2010) Regulation of divalent metal transporter 1 (DMT1) non-IRE isoform by the microRNA Let-7d in erythroid cells. Haematologica 95:1244–1252

Arosio P, Ingrassia R, Cavadini P (2009) Ferritins: a family of molecules for iron storage, antioxidation and more. Biochim Biophys Acta 1790:589–599

Bao G, Clifton M, Hoette TM, Mori K, Deng SX, Qiu A, Viltard M, Williams D, Paragas N, Leete T, Kulkarni R, Li X, Lee B, Kalandadze A, Ratner AJ, Pizarro JC, Schmidt-Ott KM, Landry DW, Raymond KN, Strong RK, Barasch J (2010) Iron traffics in circulation bound to a siderocalin (Ngal)–catechol complex. Nat Chem Biol 6:602–609

Breuer W, Epsztejn S, Cabantchik ZI (1995) Iron acquired from transferrin by K562 cells is delivered into a cytoplasmic pool of chelatable iron(II). J Biol Chem 271:24209–24215

Breuer W, Shvartsman M, Cabantchik ZI (2008) Intracellular labile iron. Int J Biochem Cell Biol 40:350–354

Crook TR, Souhami RL, Whyman GD, McLean AEM (1986) Glutathione depletion as a determinant of human leukemia cells to cyclophosphamide. Cancer Res 46:5035–5038

Devireddy LR, Hart DO, Goetz DH, Green MR (2010) A mammalian siderophore synthesized by an enzyme with a bacterial homolog involved in enterobactin production. Cell 141:1006–1017

Epzstejn S, Kakhlon O, Glickstejn H, Breuer W, Cabantchik ZI (1997) Fluorescence analysis of the labile iron pool of mammalian cells. Anal Biochem 248:31–40

Guo K, Lukacik P, Papagrigoriou E, Meier M, Lee WH, Adamski J, Oppermann U (2006) Characterization of human DHRS6, an orphan short chain dehydrogenase/reductase enzyme: a novel, cytosolic type 2 R-beta-hydroxybutyrate dehydrogenase. J Biol Chem 281:10291–10297

Hider RC, Kong XL (2011) Glutathione: a key component of the cytoplasmic labile iron pool. Biometals 24:1179–1187

Kakhlon O, Cabantchik ZI (2002) The labile iron pool: characterization, measurement and participation in cellular processes. Free Radic Biol Med 33:1037–1046

Kakhlon O, Manning H, Breuer W, Melamed-Book N, Lu C, Cortopassi G, Munnich A, Cabantchik ZI (2008) Cell functions impaired by frataxin deficiency are restored by drug-mediated iron relocation. Blood 112:5219–5227

Klausner RD, Van Renswoude J, Ashwell G, Kempf C, Schechter AN, Dean A, Bridges KR (1983) Receptor-mediated endocytosis of transferrin in K562 cells. J Biol Chem 258:4715–4724

Lane DJR, Lawen A (2008) Non-transferrin iron reduction and uptake are regulated by transmembrane ascorbate cycling in K562 cells. J Biol Chem 283:12701–12708

Lange H, Kispal G, Lill R (1999) Mechanism of iron transport to the site of heme synthesis inside yeast mitochondria. J Biol Chem 274:18989–18996

Liuzzi JP, Aydemir F, Nam H, Knutson MD, Cousins RJ (2006) Zip14 (Slc39a14) mediates non-transferrin-bound iron uptake into cells. PNAS USA 103:13612–13617

Machida K, Ohta Y, Osada H (2006) Suppression of apoptosis by cyclophilin D via stabilization of hexokinase II mitochondrial binding in cancer cells. J Biol Chem 281:14314–14320

McKie AT (2005) A ferrireductase fills the gap in the transferrin cycle. Nat Genet 37:1159–1160

Mühlenhoff U, Richhardt N, Gerber J, Lill R (2002) Characterization of iron–sulfur protein assembly in isolated mitochondria. A requirement for ATP, NADH, and reduced iron. J Biol Chem 277:29810–29816

Mühlenhoff U, Molik S, Godoy JR, Uzarska MA, Richter N, Seubert A, Zhang Y, Stubbe J, Pierrel F, Herrero E, Lillig CH, Lill R (2010) Cytosolic monothiol glutaredoxins function in intracellular iron sensing and trafficking via their bound iron-sulfur cluster. Cell Metab 12:373–385

Munujos P, Coll-Canti J, Gonzalez-Sastre F, Gella FJ (1993) Assay of succinate dehydrogenase activity by a colorimetric-continuous method using iodonitrotetrazolium chloride as electron acceptor. Anal Biochem 212:506–509

Nishikawa M, Nojima S, Akiyama T, Sankawa U, Inoue K (1984) Interaction of digitonin and its analogs with membrane cholesterol. J Biochem (Tokyo) 96:1231–1239

Paradkar PN, Zumbrennen KB, Paw BH, Ward DM, Kaplan J (2009) Regulation of mitochondrial iron import through differential turnover of mitoferrin 1 and mitoferrin 2. Mol Cell Biol 29:1007–1016

Petrat F, Weisheit D, Lensen M, de Groot H, Sustmann R, Rauen U (2002) Selective determination of mitochondrial chelatable iron in viable cells with a new fluorescent sensor. Biochem J 362:137–147

Rahman I, Kode A, Biswas SK (2006) Assay for quantitative determination of glutathione and glutathione disulfide levels using enzymatic recycling method. Nat Protoc 1:3159–3165

Shalev O, Hebbel RP (1996) Extremely high affinity association of Fe(III) with the sickle cell red membrane. Blood 88:349–352

Shaw GC, Cope JJ, Li L, Corson K, Hersey C, Ackermann GE, Gwynn B, Lambert AJ, Wingert RA, Traver D, Trede NS, Barut BA, Zhou Y, Minet E, Donovan A, Brownlie A, Balzan R, Weiss MJ, Peters LL, Kaplan J, Zon LI, Paw BH (2006) Mitoferrin is essential for erythroid iron assimilation. Nature 440:96–100

Sheftel AD, Lill R (2009) The power plant of the cell is also a smithy: the emerging role of mitochondria in iron homeostasis. Ann Med 41:82–89

Sheftel AD, Zhang AS, Brown C, Shirihai OS, Ponka P (2007) Direct interorganellar transfer of iron from endosome to mitochondrion. Blood 110:125–132

Shi H, Bencze KZ, Stemmler TL, Philpott CC (2008) A cytosolic iron chaperone that delivers iron to ferritin. Science 320:1207–1210

Shvartsman M, Kikkeri R, Shanzer A, Cabantchik ZI (2007) Non-transferrin-bound iron reaches mitochondria by a chelator-inaccessible mechanism: Biological and clinical implications. Am J Physiol Cell Physiol 293:C1383–C1394

Shvartsman M, Fibach E, Cabantchik ZI (2010) Transferrin-iron routing to the cytosol and mitochondria as studied by live and real-time fluorescence. Biochem J 429:185–193

Wang J, Pantopoulos K (2011) Regulation of cellular iron metabolism. Biochem J 434:365–381

Weaver J, Pollack S (1989) LoW-Mr iron isolated from guinea pig reticulocytes as AMP-Fe and ATP-Fe complexes. Biochem J 261:787–792

Weaver J, Pollack S (1990) Two types of receptors for iron on mitochondria. Biochem J 271:463–466

Weaver J, Pollack S, Zhan H (1989) Low molecular weight iron from guinea pig reticulocytes isolated by Sephadex G25 chromatography. Eur J Haematol 43:321–327

Weaver J, Zhan H, Pollack S (1990) Mitochondria have Fe(III) receptors. Biochem J 265:415–419

Zhan H, Gupta RK, Weaver J, Pollack S (1990) Iron bound to low MW ligands: interactions with mitochondria and cytosolic proteins. Eur J Haematol 44:124–130

Zhao N, Gao J, Enns CA, Knutson MD (2010) ZRT/IRT-like protein 14 (ZIP14) promotes the cellular assimilation of iron from transferrin. J Biol Chem 285:32141–32150